Journal of Alloys and Compounds 575 (2013) 233–238

Contents lists available at SciVerse ScienceDirect

Journal of Alloys and Compounds

journal homepage: www.elsevier.com/locate/jalcom

A comparative study on electroluminescence from ZnO-based double heterojunction light emitting diodes grown on different lattice mismatch substrates

Yongfeng Li [a,b], Bin Yao [b,c,*], Rui Deng [d], Binghui Li [b], Zhenzhong Zhang [b], Chongxin Shan [b], Dongxu Zhao [b], Dezhen Shen [b]

[a] Key Laboratory of Physics and Technology for Advanced Batteries (Ministry of Education), College of Physics, Jilin University, Changchun 130012, People's Republic of China
[b] State Key Laboratory of Luminescence and Applications, Changchun Institute of Optics, Fine Mechanics and Physics, Chinese Academy of Sciences, No. 3888 Dongnanhu Road, Changchun 130033, People's Republic of China
[c] State Key Lab of Superhard Material, and College of Physics, Jilin University, Changchun 130012, People's Republic of China
[d] School of Materials Science and Engineering, Changchun University of Science and Technology, Changchun 130022, People's Republic of China

ARTICLE INFO

Article history:
Received 23 December 2012
Received in revised form 4 April 2013
Accepted 6 April 2013
Available online 23 April 2013

Keywords:
Light-emitting diode
ZnO
Lattice mismatch
Molecular beam epitaxy

ABSTRACT

We have comparatively investigated the electroluminescence (EL) performance from the asymmetric *p*-$Mg_{0.05}Zn_{0.95}O$/*i*-ZnO/n^+-GaN and *p*-$Mg_{0.05}Zn_{0.95}O$/*i*-ZnO/n^+-Si double-heterojunction light emitting diodes (LEDs) grown on different lattice mismatch substrates. The *I–V* curve measurements show clear rectification characteristics with a threshold voltage of 3.8 and 6 V for the *p*-$Mg_{0.05}Zn_{0.95}O$/*i*-ZnO/n^+-GaN and *p*-$Mg_{0.05}Zn_{0.95}O$/*i*-ZnO/n^+-Si double heterojunctions, respectively. A strong violet-ultraviolet EL emission and no deep-level emission were observed for the *p*-$Mg_{0.05}Zn_{0.95}O$/*i*-ZnO/n^+-GaN double heterojunction grown on small lattice-mismatched n^+-GaN substrate. In comparison, a dominant visible emission band and a weak ultraviolet emission peak were observed for *p*-$Mg_{0.05}Zn_{0.95}O$/*i*-ZnO/n^+-Si double heterojunction grown on large lattice-mismatched n^+-Si substrate. The difference between both LEDs is due to different quality of the MgZnO and ZnO layers grown on different lattice mismatch substrates.

1. Introduction

Recent decades, functional metal oxides have been exclusively studied and rapidly developed due to their wide varieties of applications in the current electronic industry [1]. Such metal oxides with interesting, novel and useful properties are driving more research in chemistry, physics, and materials science. Some wide band gap oxides, involving ZnO, SnO_2, TiO_2, In_2O_3, etc. have been extensively applied in the fields of gas sensors, transparent conducting thin films, catalysis, solar cells and so on [2–9]. In the field of short-wavelength semiconductor light-emitting diodes (LEDs) and laser diodes (LDs), ZnO has received much attention for its potential applications in the field due to wide direct band gap of 3.37 eV and high exciton binding energy (60 meV) [10–12]. Although some groups have recently reported the electroluminescence (EL) from ZnO-based LEDs even demonstrated electrically pumped ZnO laser [13–20], some difficulties have been severely constrains the optoelectronic application of ZnO-based materials. These difficulties can be summarized as follows: (i) the lack of lattice-matched substrate badly suppresses crystal quality of ZnO thin films and (ii) the inherent difficulties of fabricating reproducible, reliable, stable and high-quality *p*-type ZnO hinder the application of ZnO-based homojunction [21–23]. To address the first problem, it is an effective route to find small lattice-matched substrates. Although $ScAlMgO_4$ (SCAM) is a suitable substrate material due to excellent lattice-matched condition, SCAM is an expensive compound and it is difficult to grow large crystal [24]. Among the some crystals with wurtzite structure, gallium nitride (GaN), owing to the same crystalline structure, small lattice-mismatch and thermal mismatch with ZnO, has been considered as a good choice to fabricate ZnO-based heterojunction LEDs [25]. For the second problem, some researchers adopted co-doped method to overcome low acceptor solution. For example, Gai et al. proposed theoretically that employing Mg alloyed into N doped ZnO can increase N solution and obtain *p*-type MgZnO:N. Nakahara et al. realized experimentally *p*-type MgZnO:N alloy film using molecular beam epitaxy (MBE) and observed electrically pumped UV light emission from p-MgZnO:N/ZnO heterojunctions [26]. Recently, our group also obtained *p*-type MgZnO alloy films [27–31]. Meanwhile, the *p*-type MgZnO alloy has another advantage, for example, utilizing MgZnO as barrier layer, it is easy to fabricate ZnO-based heterostructures, such as quantum well, double heterojuction,

* Corresponding author at: State Key Lab of Superhard Material, and College of Physics, Jilin University, Changchun 130012, People's Republic of China.
E-mail address: binyao@jlu.edu.cn (B. Yao).

0925-8388/$ - see front matter © 2013 Elsevier B.V. All rights reserved.
http://dx.doi.org/10.1016/j.jallcom.2013.04.036

for effective confining carriers in well layers or interfaces [26,32–36].

On the other hand, it is expected that ZnO-based LEDs have good EL performance, in which ultraviolet (UV) light emission relevant to exciton recombination is dominant. However, strong visible emission is usually observed in ZnO-based LED with a poor crystal quality. The defects related to deep levels give rise to the visible emission and they are easily formed in ZnO. Therefore, high quality ZnO films with low-density defects are important for obtaining ZnO-based LED with high performance.

Here we demonstrate two kinds of asymmetry ZnO-based double heterojunctions grown on *n*-type GaN and Si substrates with lattice-mismatch of 2% and 15%, respectively. A dominant UV EL was observed in the *p*-MgZnO/*i*-ZnO/n^+-GaN double-heterostructure LED with small lattice-match. In contrast, the large lattice-matched *p*-MgZnO/*i*-ZnO/n^+-Si LED shows a strong visible emission band and a weak UV emission peak.

2. Experimental details

The heavily doped *n*-type GaN (0 0 1)/sapphire and Si (1 1 1) wafer with electron concentration of $\sim 10^{19}$ cm^{-3} as substrates were together put in MBE growth chamber. First, an undoped ZnO thin film with a thickness of 50 nm was fabricated on the n^+-GaN and n^+-Si substrates at 800 °C. The ZnO thin films were annealed *in situ* at 850 °C in the activated oxygen atom atmosphere to improve crystal quality. Then, a 500-nm-thick nitrogen-doped *p*-type MgZnO (MgZnO:N) alloy thin film was grown on the ZnO layer at 450 °C. During the growth process, the 6 N-pure metal Zn and Mg were used as the Zn and Mg source. The highly pure O_2 and N_2 gas (5 N in purity) were activated by two Oxford Applied Research Model HD25 rf (13.56 MHz) atomic sources, respectively. The metal Ni/Au alloy was sequentially evaporated on the *p*-type MgZnO:N layer. To obtain ohmic contact of Ni/Au to *p*-type layer, a annealing was performed at 350 °C for 15 min in air. For the *n*-type contact electrodes, the metal indium was sintered on the n^+-GaN and n^+-Si substrates at a vacuum chamber. The schematic structures of the asymmetry *p*-MgZnO/*i*-ZnO/n^+-GaN and *p*-MgZnO/*i*-ZnO/n^+-Si double-heterostructure LEDs are shown in Fig. 3a and b, respectively.

The electrical properties and *I–V* curves of the samples were characterized with a Lakeshore 7707 Hall system. The Hall effect measurement was performed in a van der Pauw configuration. The surface morphology and roughness of the films was characterized by atomic force microscopy (AFM). To determine the Mg and N composition in the N-doped MgZnO alloy film, X-ray photoelectron spectroscopy (XPS) measurement was performed using an ESCALAB 250 XPS instrument with Al Kα ($h\nu$ = 1486.6 eV) X-ray radiation source. The XPS spectra were calibrated by the C 1*s* peak (284.6 eV). The Raman spectroscopy and photoluminescence (PL) were measured using 488 nm line of Ar^+ laser and 325 nm line of He–Cd laser as excitation sources, respectively. EL measurements were performed using a Hitachi F4500 spectrometer and a current power source as an excite source.

3. Results and discussion

3.1. Raman spectroscopy and morphology characterization of ZnO films grown GaN and Si

To characterize the crystal quality and stress states of the ZnO films on the GaN and Si substrates (here denoted as ZnO/GaN and ZnO/Si films), we also fabricated the ZnO films on both GaN and Si substrates at the same growth condition of the double heterojunction LEDs. Raman spectroscopy measurements were performed for characterizing stress state of the epitaxial ZnO films. A bulk ZnO was also measured for comparison. As shown in Fig. 1a, for the bulk ZnO, the E_2 (high) mode is located at 437 cm^{-1}, which is consistent with the results previously reported [37,38]. Importantly, the mode E_2 (high) peaks are located

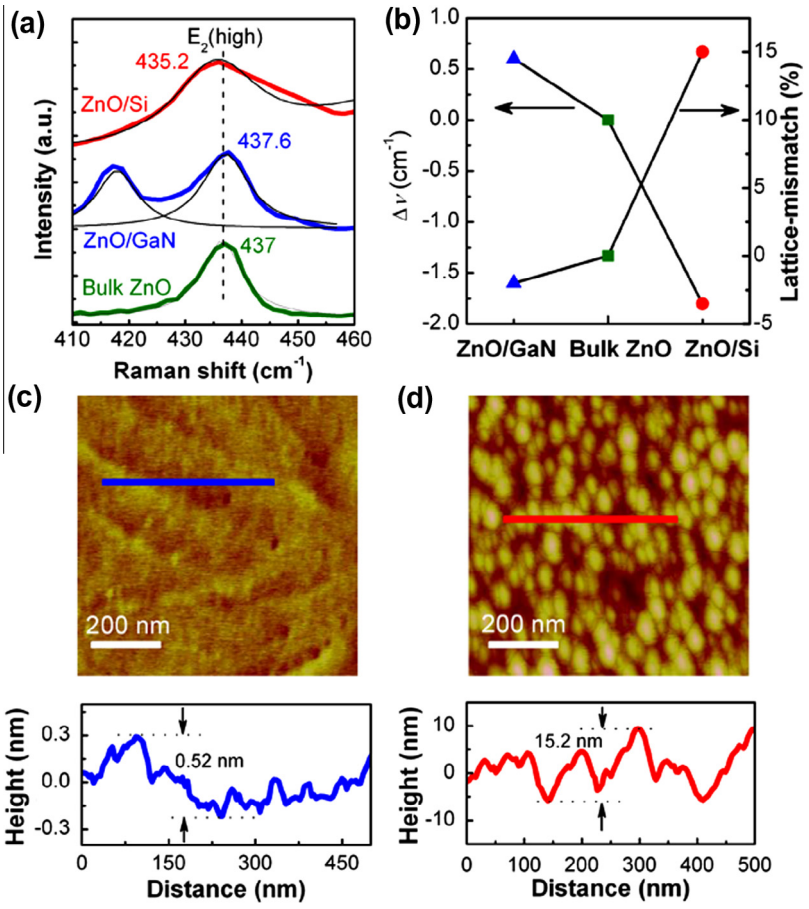

Fig. 1. (a) E_2 (high) modes in Raman spectroscopy of the bulk ZnO, ZnO/*n*-GaN and ZnO/*n*-Si thin films. (b) The lattice-mismatch of the ZnO/*n*-GaN and ZnO/*n*-Si as well as their E_2 (high) modes shift with respect to bulk ZnO. AFM images of the surfaces for the (c) ZnO/*n*-GaN and (d) ZnO/*n*-Si as well as corresponding step heights.

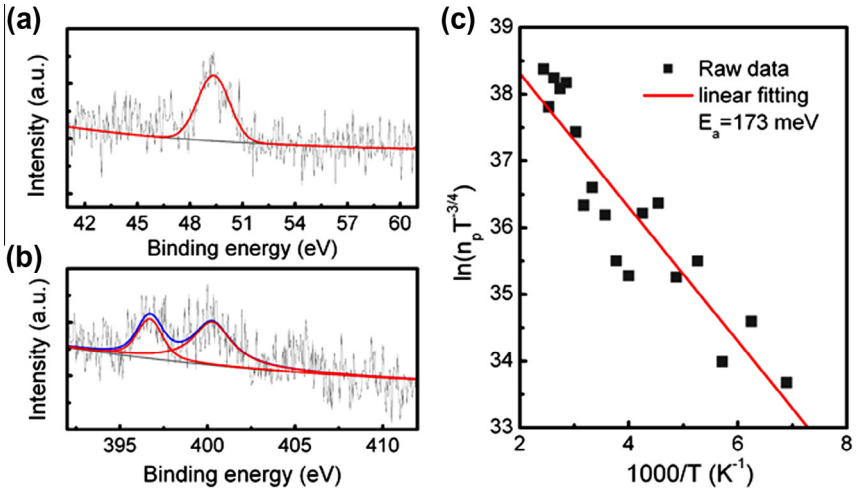

Fig. 2. XPS spectra of (a) Mg-2*p* and (b) N-1*s* states of the *p*-type $Mg_xZn_{1-x}O$ alloy thin film. (c) The plot of $\ln(n_pT^{3/4})$ as a function of $1/T$ for the *p*-type $Mg_xZn_{1-x}O$ alloy thin film.

at 437.6 and 435.2 cm^{-1} for the ZnO/GaN and ZnO/Si films, respectively. For the ZnO/GaN film, a small Raman shift of 0.6 cm^{-1} toward large wavenumber indicates the ZnO film is slightly subjected to compressive stress. However, for the ZnO/Si film, there is a significant Raman shift (−1.8 cm^{-1}) with respect to the bulk ZnO, indicating that large tensile stresses are in the ZnO film grown on Si substrate. These results can be well explained by lattice-mismatch between film and substrate. Both GaN (001) and Si (111) have the same structure with wurtzite ZnO (001). In this case, we can calculate their lattice-mismatch. The lattice-mismatch between ZnO film and substrate can be expressed as $(a_{sub} - a_{ZnO})/a_{sub}$, where a_{sub} and a_{ZnO} are lattice constant in substrate and film plane, respectively. The calculated lattice-mismatch of ZnO/GaN and ZnO/Si (111) is −2% and 15%, respectively. The negative sign represents lattice constant of substrate is smaller than ZnO films. The large lattice-mismatch of ZnO/Si leads to the large tensile stress. Furthermore, according to literatures reported, (001) preferred orientation is observed in XRD patterns for the ZnO films grown on GaN and Si (111) substrates [39,40]. However, for ZnO film grown on Si (111), ZnO film are rotated by 30° with respect to the Si (111) substrate orientation. However, For the ZnO film grown on GaN, there is not such rotation due to small lattice-mismatch. The 30° rotation of ZnO with respect to Si (111) usually leads to more defects and lowers ZnO film quality. Fig. 1b shows the E_2 (high) mode shift of the ZnO films and lattice-mismatch of substrates with respect to bulk ZnO. For further comparing the surface roughness of both ZnO films, the atomic force microscopy (AFM) measurements were carried out. Fig. 1c and d shows the AFM images of the ZnO/GaN and ZnO/Si films, respectively. The ZnO/GaN film shows an almost atomically flat with a step height of 0.52 nm, much smoother than the ZnO/Si film, indicating ZnO/GaN film has higher crystal quality. The smooth surface of the ZnO/GaN film ensures that the subsequently fabricated *p*-type MgZnO:N layer is reliable and high-quality. In general, as a film is epitaxially grown on lattice-mismatched substrate, stress is introduced into the film. The stress cannot be accumulated continuously during the film growth process and it can be released or partially released through forming defects. The defects lead to poor crystal quality. It should be noted that the lattice-mismatch of ZnO/Si (111) is much larger than ZnO/GaN and the ZnO/Si film is subjected to larger stress. As the stress is released or partially released, the defects occur in the film, resulting in a poor crystal quality and rougher surface in the ZnO/Si film.

3.2. XPS composition and electrical properties of N-doped MgZnO alloy film

Next, the MgZnO:N thin films were continuously fabricated on the *in situ* annealed ZnO layers to form double heterojunction. To avoid the effect of the ZnO layers and conducting substrates on Hall effect measurement of MgZnO:N film, the MgZnO:N film was also fabricated on sapphire at the same deposition condition. Hall effect measurement indicates that the *p*-type MgZnO:N/sapphire has a hole concentration of 5.6×10^{17} cm^{-3} and a mobility of 3.1 cm^2/vs. To further determine the Mg and N content in the *p*-type MgZnO:N alloy films, XPS measurement was performed. Fig. 2a and b shows the XPS spectra of Mg 2*p* and N 1*s* states of the *p*-type $Mg_xZn_{1-x}O$:N alloy film. The Mg content (x) in the *p*-type $Mg_xZn_{1-x}O$ alloy is determined to be 0.05. The N 1*s* spectrum reveals two distinct peaks at 396.6 and 400.3 eV. The binding energy of N 1*s* line can vary from 395 to 408 eV due to different chemical environment of nitrogen atom [41]. The peak at 396.6 eV is assigned to nitrogen substitution at oxygen site (N_O), acting as acceptor [42]. The peak around 400 eV has been assigned to the C–N component [43]. The C–N bond originates from chemical reaction between N and absorbed C or CO_2 on the surface of the MgZnO thin film. It is reported that the peak at about 405 eV is considered to be related to molecular N_2 substitution at oxygen site [$(N_2)_O$], acting as donor [44]. It should be noted that no distinct peak is observed at ~405 eV in the present work, implying the formation of the effective *p*-type MgZnO.

To further investigate the acceptor ionization energy in the *p*-type MgZnO:N, a variable temperature Hall effect measurement was performed, as shown in Fig. 2c. The relationship between hole concentration n_p and ionization energy E_a of acceptor can be expressed as follows:

$$n_p = \sqrt{N_A N_V/2}\exp(-E_a/2k_BT) \quad (1)$$

where N_A and N_V are the acceptor impurity concentration and hole effective density of states of valence band, respectively. The k_B and T are Boltzmann constant and temperature. Due to $N_V \propto T^{3/2}$, Eq. (1) can be written as follows,

$$\ln(n_pT^{3/4}) \propto -E_a/2k_BT \quad (2)$$

By fitting the data to Eq. (2), the ionization energy of the acceptor is estimated to be about 173 meV, which is higher than N-doped ZnO and lower than N-doped $Mg_{0.2}Zn_{0.8}O$ films due to the shift of va-

lence-band maximum (VBM) to low energy side as Mg alloyed into ZnO [45–47]. The result indicates that the N dopants are effective acceptors in the N-doped MgZnO alloy.

3.3. Comparatively studies on performance of p-MgZnO/i-ZnO/n^+-GaN and p-MgZnO/i-ZnO/n^+-Si double heterojunction LEDs

Fig. 3a and b shows the schematic diagrams of the *p*-MgZnO/*i*-ZnO/n^+-GaN and *p*-MgZnO/*i*-ZnO/n^+-Si double heterojunction LEDs, respectively. The *I–V* curves of both devices are shown in Fig. 3c. The turn-on voltages are 3.8 and 6 V for the *p*-MgZnO/*i*-ZnO/n^+-GaN and *p*-MgZnO/*i*-ZnO/n^+-Si double heterojunctions, respectively. The threshold voltage of 3.8 V for the *p*-MgZnO/*i*-ZnO/n^+-GaN device is slightly larger than the band gap of ZnO. The higher threshold voltages for the *p*-MgZnO/*i*-ZnO/n^+-Si device should be related to the quality of the devices. The inset of Fig. 3c show the *I–V* curves in semilogarithmic scale. The calculated rectification ratios of the *p*-MgZnO/*i*-ZnO/n^+-GaN and *p*-MgZnO/*i*-ZnO/n^+-Si are 5.5 and 4.0 at 10 V, respectively. The low rectification ratios may be ascribed to the low quality interface of *p*-MgZnO and *i*-ZnO layers. To exclude the rectification originating from Schottky contact between *p*-MgZnO and Ni/Au layers, we verified that the Ni/Au contacts to the *p*-MgZnO layer are ohmic, as shown in Fig. 3d. The ohmic contacts of the indium electrodes to n^+-GaN and n^+-Si are also shown in Fig. 3d.

Fig. 4a shows the EL spectra of the *p*-MgZnO/*i*-ZnO/n^+-GaN heterojunction at the injection current of 1.5, 3.5 and 5.5 mA, respectively. In these EL spectra, there is an emission band in a range from violet to UV region, but no emission related to deep level, indicating that the LED has a good performance. For clarifying the origin of the EL emission band from violet to UV, we measured the PL spectra of the ZnO, GaN and MgZnO/ZnO films grown on sapphire substrates under the corresponding condition of fabricating heterojunction, respectively, as shown in Fig. 4b. The PL spectra of the ZnO and GaN reveal sharp PL emission peak at 3.3 and 3.42 eV, which is ascribed to the radiative recombination of free-exciton in ZnO and near band edge in GaN, respectively. These results indicate that both ZnO and GaN layers have high photoluminescence quality. However, for the MgZnO/ZnO film, there exist two distinct peaks in the PL spectrum. The strong and weak peaks are located at about 3 and 3.39 eV, respectively. The peak at 3.39 eV is attributed to the near-band-edge (NBE) of the MgZnO alloy. The emission at about 3 eV is related to defects. There may be two main factors leading to the emission at 3 eV: (i) the recombination of donor–acceptor pair (DAP) in the *p*-MgZnO layer due to N doping and (ii) defects induced by lattice-mismatch at the *p*-MgZnO/ZnO interface. Meanwhile, the EL emission band covers the range of 3–3.3 eV, involving the emissions of NBE (3.2–3.3 eV) and defects (~3 eV). Thus, it is reasonable that the emission band is fitted to two peaks. The inset of Fig. 4a shows the Gaussian fitting result of the EL emission band at the injection current of 5.5 mA. One fitting peak is at 3 eV and the other is at about 3.25 eV. Combined with the PL spectra, it is deduced that the EL emissions at 3 eV originates from the *p*-MgZnO layer or *p*-MgZnO/ZnO interface, and the emission at 3.25 eV originates from the ZnO layer. At low injection current, the peak at about 3 eV is much stronger than the one at 3.25 eV. The intensity of the peak at 3.25 eV increases with the increase of the injection current. As the injection current is 5.5 mA, the peak at 3.25 eV is dominant. Therefore, it is deduced that the increase of the injection current can improve the quality of the EL emission in the UV region.

The EL spectra of the *p*-MgZnO/*i*-ZnO/n^+-Si double heterojunction are shown in Fig. 4c. It is observed there is a strong emission band at the visible region and a weak violet-UV emission peak in the EL spectra. The result is significantly different from the *p*-MgZnO/*i*-ZnO/n^+-GaN heterojunction. To clarify the origin of the EL, we also performed the PL measurement for the *p*-MgZnO/*i*-ZnO/n^+-Si double heterojunction, as shown in Fig. 4d. Similar with the EL spectra, there is also a strong visible emission band and a weak violet-UV emission peak. It is deduced that the weak peak at ~3 eV should be the same origin with the *p*-MgZnO/*i*-ZnO/n^+-GaN heterojunction. The strong emission band at ~2.5 eV is attrib-

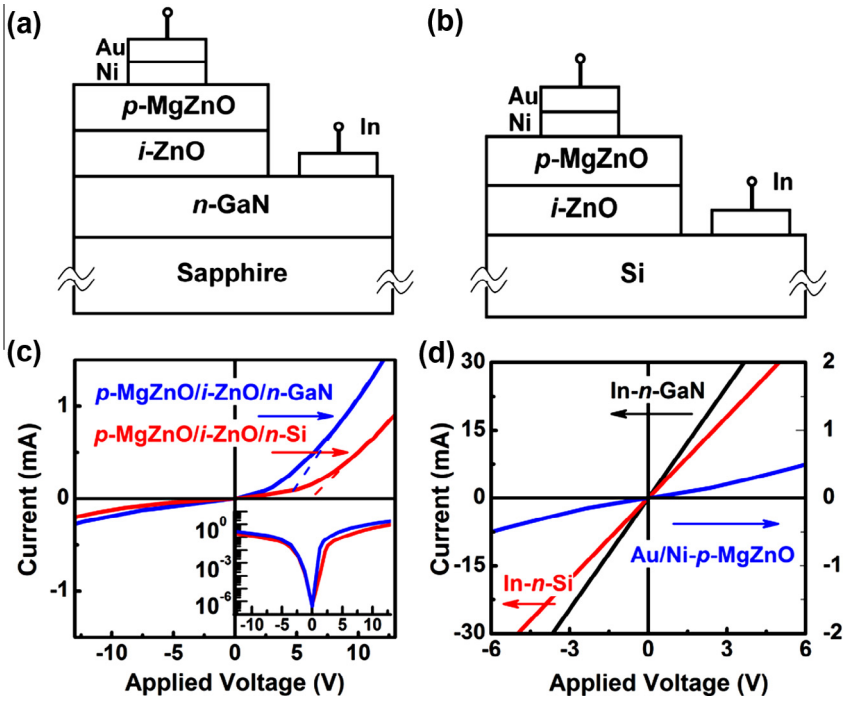

Fig. 3. Schematic diagrams of device structures of (a) *p*-MgZnO/*i*-ZnO/n^+-GaN and (b) *p*-MgZnO/*i*-ZnO/n^+-Si double heterostructures. (c) Room temperature *I–V* characteristics of *p*-MgZnO/*i*-ZnO/n^+-GaN and *p*-MgZnO/*i*-ZnO/n^+-Si double heterostructural LEDs. The threshold voltages are 3.8 and 6 V for the *p*-MgZnO/*i*-ZnO/n^+-GaN and *p*-MgZnO/*i*-ZnO/n^+-Si devices. The inset shows the *I–V* curves in semilogarithmic scale. (d) Ohmic contact characteristics of the In-*n*-GaN, In-*n*-Si and Au/Ni-*p*-MgZnO.

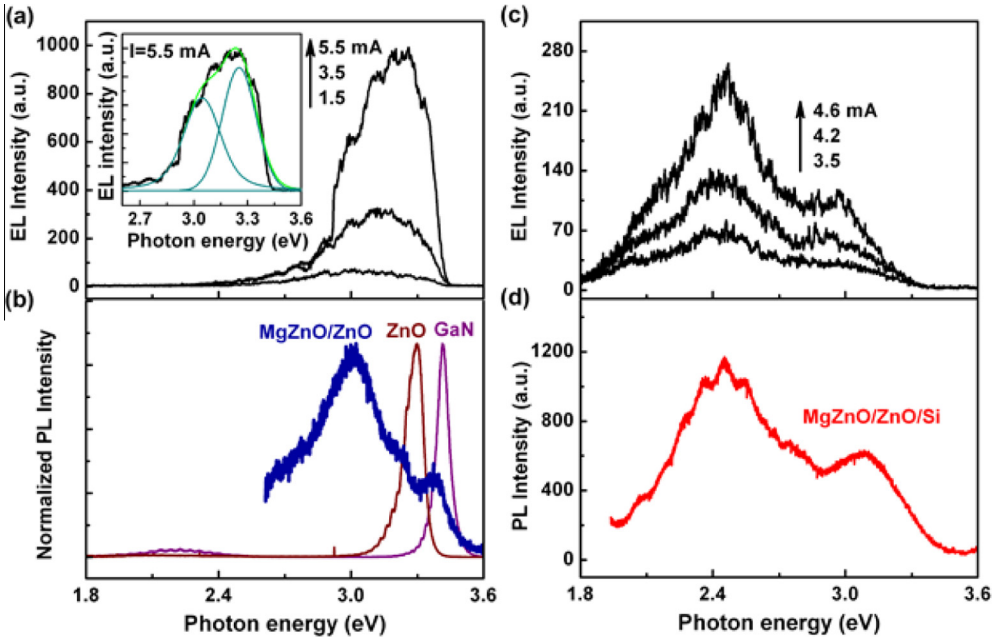

Fig. 4. RT EL and PL spectra of the (a), (b) *p*-MgZnO/*i*-ZnO/n^+-GaN and (c), (d) *p*-MgZnO/*i*-ZnO/n^+-Si double heterojunction LEDs.

uted to the radiative recombination of deep level defects from the ZnO or MgZnO layers. The EL difference between both devices results from different quality of the MgZnO/ZnO layers grown on different lattice mismatch substrates.

In order to further elucidate the origin of the EL difference, the schematic diagrams of band alignments in the *p*-MgZnO/*i*-ZnO/n^+-GaN and the *p*-MgZnO/*i*-ZnO/n^+-Si double heterojunctions under a forward bias are illustrated in Fig. 5a and b, respectively. The ratio of the conduction-band offset (CBO) to valance-band offset (VBO) at the interface of MgO/ZnO heterojunction is calculated to be about 4 according to the electron affinity and band gap of MgO and ZnO, in good agreement with the XPS measurement result [47]. The band gap of $Mg_{0.05}Zn_{0.95}O$ alloy is estimated to be 0.1 eV larger than that of ZnO according to the relation between band gap and Mg content [48]. Thus, the CBO and VBO at the interface of the $Mg_{0.05}Zn_{0.95}O$/ZnO heterojunction are estimated to be 0.08 and 0.02 eV by linear extrapolation, respectively. Similarly, the CBO and VBO at the interface of the ZnO/GaN heterojunction are determined to be 0.15 and 0.09 eV, respectively. For the ZnO/Si interface, the CBO and VBO are estimated to be 0.2 and 2.45 eV, respectively. In this case, electrons can be confined in the ZnO layer due to the electron barriers at the both interfaces of the double-heterostructures. As a forward bias is applied to the LEDs, holes from the MgZnO layers and electrons from the GaN or Si layer are injected into the ZnO layer, in which radiative recombination of electrons and holes happens. Thus, the quality of the ZnO layer determines the performance of the EL. The high quality of ZnO layer grown on the small lattice-mismatched GaN substrate gives rise to a good emission performance. Oppositely, the poor quality of ZnO layer grown on the large lattice-mismatched Si substrate leads to the strong visible emission.

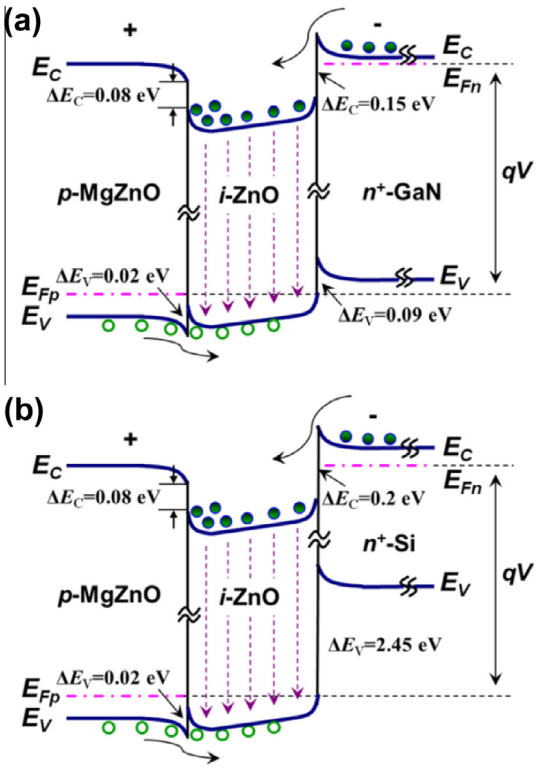

Fig. 5. Schematic diagrams of energy bands of (a) *p*-$Mg_{0.05}Zn_{0.95}O$/*i*-ZnO/n^+-GaN and (b) *p*-$Mg_{0.05}Zn_{0.95}O$/*i*-ZnO/n^+-Si double heterostructures at forward bias voltage.

4. Conclusions

We have comparatively investigated the EL performance of the *p*-$Mg_{0.05}Zn_{0.95}O$/*i*-ZnO/n^+-GaN and *p*-$Mg_{0.05}Zn_{0.95}O$/*i*-ZnO/n^+-Si double heterojunction LEDs grown on different lattice-mismatched substrates. The *I–V* curve measurements show clear rectification characteristics with a threshold voltage of 3.8 and 6 V for the *p*-$Mg_{0.05}Zn_{0.95}O$/*i*-ZnO/n^+-GaN and *p*-$Mg_{0.05}Zn_{0.95}O$/*i*-ZnO/n^+-Si double heterojunctions, respectively. Both LEDs shows different EL performance. A strong violet-UV EL emission and no deep level related emission were observed for the *p*-$Mg_{0.05}Zn_{0.95}O$/*i*-ZnO/n^+-GaN double heterojunction. In comparison, a dominant visible emission band and a weak UV emission peak were observed for *p*-$Mg_{0.05}Zn_{0.95}O$/*i*-ZnO/n^+-Si double heterojunction. The difference

between both LEDs is due to different quality of the MgZnO and ZnO layers grown on different lattice mismatch substrates.

Acknowledgments

This work was supported by the National Natural Science Foundation of China under Grant Nos. 10874178, 11074093, 61205038, and 11274135, Natural Science Foundation of Jilin province under Grant No. 201115013, National Found for Fostering Talents of Basic Science under Grant No. J1103202, Ph.D. Programs Foundation of Ministry of Education of China under Granted No. 20120061120011.

References

[1] D.W. Bruce, D. O'Hare, R.I. Walton, Functional Oxides, Wiley, 2011.
[2] Z. Chen, S. Li, W. Zhang, J. Alloys Comp. 557 (2013) 274.
[3] K. Jung, W.-K. Choi, K.H. Chae, J.-H. Song, S.-J. Yoon, M.-H. Lee, J.-W. Choi, J. Alloys Comp. 554 (2013) 240.
[4] N.M.A. Hadia, H.A. Mohamed, J. Alloys Comp. 547 (2013) 63.
[5] P. Biswas, S. Kundu, P. Banerji, J. Alloys Comp. 552 (2013) 304.
[6] R. Vyas, S. Sharma, P. Gupta, Y.K. Vijay, A.K. Prasad, A.K. Tyagi, K. Sachdev, S.K. Sharma, J. Alloys Comp. 554 (2013) 59.
[7] Y. Li, R. Deng, Y. Tian, B. Yao, T. Wu, Appl. Phys. Lett. 100 (2012) 172402.
[8] Y. Li, W. Yin, R. Deng, R. Chen, J. Chen, Q. Yan, B. Yao, H. Sun, S.-H. Wei, T. Wu, NPG Asia Mater. 4 (2012) e30.
[9] Z. Liu, X. Su, G. Hou, S. Bi, Z. Xiao, H. Jia, J. Alloys Comp. 555 (2013) 68.
[10] D.C. Look, Mater. Sci. Eng. B: Solid 80 (2001) 383.
[11] Z.K. Tang, G.K.L. Wong, P. Yu, M. Kawasaki, A. Ohtomo, H. Koinuma, Y. Segawa, Appl. Phys. Lett. 72 (1998) 3270.
[12] S. Nakamura, Science 281 (1998) 956.
[13] A. Tsukazaki, A. Ohtomo, T. Onuma, M. Ohtani, T. Makino, M. Sumiya, K. Ohtani, S.F. Chichibu, S. Fuke, Y. Segawa, H. Ohno, H. Koinuma, M. Kawasaki, Nat. Mater. 4 (2005) 42.
[14] S.J. Jiao, Z.Z. Zhang, Y.M. Lu, D.Z. Shen, B. Yao, J.Y. Zhang, B.H. Li, D.X. Zhao, X.W. Fan, Z.K. Tang, Appl. Phys. Lett. 88 (2006) 031911.
[15] Z.P. Wei, Y.M. Lu, D.Z. Shen, Z.Z. Zhang, B. Yao, B.H. Li, J.Y. Zhang, D.X. Zhao, X.W. Fan, Z.K. Tang, Appl. Phys. Lett. 90 (2007) 042113.
[16] Y.R. Ryu, J.A. Lubguban, T.S. Lee, H.W. White, T.S. Jeong, C.J. Youn, B.J. Kim, Appl. Phys. Lett. 90 (2007) 131115.
[17] S. Chu, M. Olmedo, Z. Yang, J. Kong, J. Liu, Appl. Phys. Lett. 93 (2008) 181106.
[18] F. Sun, C.X. Shan, B.H. Li, Z.Z. Zhang, D.Z. Shen, Z.Y. Zhang, D. Fan, Opt. Lett. 36 (2011) 499.
[19] P.-H. Lei, M.-J. Ding, Y.-C. Lee, M.-J. Chung, J. Alloys Comp. 509 (2011) 6152.
[20] S.A.M. Lima, M.R. Davolos, C. Legnani, W.G. Quirino, M. Cremona, J. Alloys Comp. 418 (2006) 35.
[21] B.Y. Zhang, B. Yao, Y.F. Li, A.M. Liu, Z.Z. Zhang, B.H. Li, G.Z. Xing, T. Wu, X.B. Qin, D.X. Zhao, C.X. Shan, D.Z. Shen, Appl. Phys. Lett. 99 (2011) 182503.
[22] B.Y. Zhang, B. Yao, Y.F. Li, Z.Z. Zhang, B.H. Li, C.X. Shan, D.X. Zhao, D.Z. Shen, Appl. Phys. Lett. 97 (2010) 222101.
[23] G.Z. Xing, Y.H. Lu, Y.F. Tian, J.B. Yi, C.C. Lim, Y.F. Li, G.P. Li, D.D. Wang, B. Yao, J. Ding, Y.P. Feng, T. Wu, AIP Adv. 1 (2011) 022152.
[24] A. Tsukazaki, A. Ohtomo, S. Yoshida, M. Kawasaki, C.H. Chia, T. Makino, Y. Segawa, T. Koida, S.F. Chichibu, H. Koinuma, Appl. Phys. Lett. 83 (2003) 2784.
[25] W.W. Liu, B. Yao, B.H. Li, Y.F. Li, J. Zheng, Z.Z. Zhang, C.X. Shan, J.Y. Zhang, D.Z. Shen, X.W. Fan, Solid State Sci. 12 (2010) 1567.
[26] K. Nakahara, S. Akasaka, H. Yuji, K. Tamura, T. Fujii, Y. Nishimoto, D. Takamizu, A. Sasaki, T. Tanabe, H. Takasu, H. Amaike, T. Onuma, S.F. Chichibu, A. Tsukazaki, A. Ohtomo, M. Kawasaki, Appl. Phys. Lett. 97 (2010) 013501.
[27] Y. Li, R. Deng, B. Yao, G. Xing, D. Wang, T. Wu, Appl. Phys. Lett. 97 (2010) 102506.
[28] Y.F. Li, B. Yao, Y.M. Lu, Z.P. Wei, Y.Q. Gai, C.J. Zheng, Z.Z. Zhang, B.H. Li, D.Z. Shen, X.W. FanZ, K. Tang, Appl. Phys. Lett. 91 (2007) 232115.
[29] Y.F. Li, B. Yao, R. Deng, B.H. Li, J.Y. Zhang, Y.M. Zhao, D.Y. Jiang, Z.Z. Zhang, C.X. Shan, D.Z. Shen, X.W. Fan, Y.M. Lu, J. Phys. D: Appl. Phys. 42 (2009) 105102.
[30] Z.P. Wei, B. Yao, X.H. Wang, Z.Z. Zhang, Y.M. Lu, D.Z. Shen, B.H. Li, J.Y. Zhang, D.X. Zhao, X.W. Fan, Z.K. Tang, J. Mater. Res. 22 (2007) 2791.
[31] W.W. Liu, B. Yao, Y.F. Li, B.H. Li, Z.Z. Zhang, C.X. Shan, J.Y. Zhang, D.Z. Shen, X.W. Fan, J. Alloys Comp. 504 (2010) 484.
[32] M. Lange, J. Kupper, C.P. Dietrich, M. Brandt, M. Stölzel, G. Benndorf, M. Lorenz, M. Grundmann, Phys. Rev. B 86 (2012) 045318.
[33] C.-T. Chi, I.C. Cheng, J.-Z. Chen, J. Alloys Comp. 544 (2012) 111.
[34] L. Cao, L. Zhu, J. Jiang, Y. Li, Y. Zhang, Z. Ye, J. Alloys Comp. 516 (2012) 157.
[35] L.Q. Zhang, Z.Z. Ye, J.Y. Huang, B. Lu, H.P. He, J.G. Lu, Y.Z. Zhang, J. Jiang, J. Zhang, K.W. Wu, W.G. Zhang, J. Alloys Comp. 509 (2011) 7405.
[36] J.D. Ye, K.W. Teoh, X.W. Sun, G.Q. Lo, D.L. Kwong, H. Zhao, S.L. Gu, R. Zhang, Y.D. Zheng, S.A. Oh, X.H. Zhang, S. Tripathy, Appl. Phys. Lett. 91 (2007) 091901.
[37] N. Ashkenov, B.N. Mbenkum, C. Bundesmann, V. Riede, M. Lorenz, D. Spemann, E.M. Kaidashev, A. Kasic, M. Schubert, M. Grundmann, G. Wagner, H. Neumann, V. Darakchieva, H. Arwin, B. Monemar, J. Appl. Phys. 93 (2003) 126.
[38] T. Damen, S. Porto, B. Tell, Phys. Rev. 142 (1966) 570.
[39] M. Fujita, N. Kawamoto, T. Tatsumi, K. Yamagishi, Y. Horikoshi, Jpn. J. Appl. Phys. 42 (2003) 67.
[40] A. Nahhas, H.K. Kim, J. Blachere, Appl. Phys. Lett. 78 (2001) 1511.
[41] X.H. Li, H.Y. Xu, X.T. Zhang, Y.C. Liu, J.W. Sun, Y.M. Lu, Appl. Phys. Lett. 95 (2009).
[42] H.Y. Wei, Y.S. Wu, L.L. Wu, C.X. Hu, Mater. Lett. 59 (2005) 271.
[43] M. Futsuhara, K. Yoshioka, O. Takai, Thin Solid Films 317 (1998) 322.
[44] C.L. Perkins, S.H. Lee, X.N. Li, S.E. AsherT, J. Coutts, J. Appl. Phys. 97 (2005).
[45] J.M. Pierce, H. Wen, K. Liu, M. Kumrr, J. Tresback, Y.S. Ali, A. Krahnert, B.T. Adekore, J Cryst. Growth 325 (2011) 20.
[46] W. Liu, S.L. Gu, J.D. Ye, S.M. Zhu, Y.X. Wu, Z.P. Shan, R. Zhang, Y.D. Zheng, S.F. Choy, G.Q. Lo, X.W. Sun, J Cryst. Growth 310 (2008) 3448.
[47] Y.F. Li, B. Yao, Y.M. Lu, B.H. Li, Y.Q. Gai, C.X. Cong, Z.Z. Zhang, D.X. Zhao, J.Y. Zhang, D.Z. Shen, X.W. Fan, Appl. Phys. Lett. 92 (2008) 192116.
[48] J. Chen, W.Z. Shen, N.B. Chen, D.J. Qiu, H.Z. Wu, J. Phys.: Condens. Matt. 15 (2003) L475.